Surface Acoustic Wave Based Microfluidics and Droplet Applications

THOMAS FRANKE*[a,b,c,e,f], THOMAS FROMMELT[d], LOTHAR SCHMID[a,e], SUSANNE BRAUNMÜLLER[a,e], TONY JUN HUANG, AND ACHIM WIXFORTH*[a,b,c,e]

[a]University of Augsburg, Augsburg, Germany; [b]Center for NanoScience, CeNS, Munich, Germany; [c]Augsburg Center for Innov. Technologies, ACIT, Augsburg, Germany; [d]SGL Carbon, Meitingen, Germany; [e]Nanosystems Initiative Munich, NIM, 80799 Munich, Germany; [f]School of Engineering, University of Glasgow, G12 8LT; [g]Department of Engineering Science and Mechanics, The Pennsylvania State University, University Park, PA 16802, USA
*E-mail: thomas.franke@glasgow.ac.uk; achim.wixforth@physik.uni-augsburg.de

16.1 Introduction

Ever since the beginning of mankind, the mastering of fluids has played an important role for modern human development. Watering and irrigation of agricultural zones was probably the first application of technological fluid handling. Later on, drinking and service water for industrial use or power generation asked for sophisticated channeling of remote water sources. Also, artificial waterways with locks for transportation of ships and goods to remote locations far from natural streams and rivers developed into an

engineering art over the centuries. Complex plumbing schemes, including pumping units, valves and containers, opened a wide area of technological advancements, which finally resulted in the highly complex water systems lancing our megacities nowadays.

On the other hand, the processing of fluids into more valuable goods required sophisticated fluid handling systems. Here, the introduction of bio- or chemo- or physical reactors such as distillation and fermentation played an important role in the development of complex fluid based goods such as wine, beer and gasoline. The development of alchemia and chemistry led to the discovery of even more complex and powerful fluid handling systems without which our modern life would be unthinkable.

In the last centuries, medical and biological applications have entered the field of fluidics, the major developments probably being the invention of dialysis or other life supporting techniques and systems.

In recent years, and probably triggered by the tremendous success of microelectronic 'chips', a new thinking in the field of fluid handling was born. Many laboratories in the world started to develop chip-sized micro-systems in which small amounts of fluids can be manipulated, such as the charges on their electronic counterparts. Sophisticated technologies for the creation of microchannels, microreactors and most importantly pumping units were created over the years. Many of them are actually based on the longstanding and proven traditions of semiconductor technology that is still improving to an unprecedented level in modern micro- and nanoelectronics, photonics and other high tech applications.

Apart from standard pumps, such as those based on capillary forces, mechanically actuated pistons, peristaltic pumping or membrane based actuators, all reduced to the microscale, electrically actuated fluid handling systems have proved very successful over the years.[1–3] Also, centrifugal forces[4] or electrical or chemical modulation of the surface energy[5] of solid substrates were shaped into real microfluidic devices. What all these devices have in common is that the fluid behavior is dictated by typically very low Reynold's numbers Re < 1. The Reynold's number basically denotes the ratio of the influence of inertia to viscosity related effects on a fluid. At low Re, typically, the apparent viscosity of the fluid dominates the streaming behavior, making actuation or even mixing a difficult task on such microfluidic chips.

16.2 Acoustic Streaming Effects

This chapter centers around the employment of acoustic fields for fluidic actuation and manipulation purposes. A sound wave propagating within a fluid and having a pressure amplitude $p_{ex}(r,t)$ larger that the static pressure p_0 may lead to a net DC flow in the liquid. It is a result of the time-averaged momentum equation and can be identified with a 'radiation pressure'. This acoustically driven fluid motion is called 'acoustic streaming', a well-known effect that has many applications and implications in hydrodynamics.

Eckart[6] and Nyborg[7] already in the 1950s gave very comprehensive analytical investigations and overviews of this effect.

A special case for the generation of acoustic streaming on a solid chip surface is the use of so-called surface acoustic waves (SAW). A SAW is a mode of elastic energy propagating at the surface of a solid, where all wave-related quantities decay in a quasi-exponential manner with depth below said surface. One of the earliest descriptions of such waves was given by Lord Rayleigh in a seminal paper on earthquakes more than a hundred years ago.[8] SAW are mainly used in high frequency filters[9] and signal processing units for mobile phone applications for example. Also, due to their high sensitivity to disturbances at the surfaces they are propagating at, SAW are widely used as sensors[10] for many different purposes. Not only are they suited to detect minute amounts of mass loading at the surface, in the case of piezoelectric substrates they are also well suited to study changes in the (di-)electric environment at or close to the surface.[11]

On piezoelectrics, SAW are especially simple to excite and detect. Here, so-called interdigital transducers (IDT) are employed to efficiently convert a high frequency electrical input signal into a travelling surface acoustic wave.[12] The geometrical layout of the IDT together with the acoustic properties of the substrate determines the SAW frequency response and wavelength. SAW can also be used to actively and acoustically transport quantities of charge within a layered (semiconductor) substrate.[13,14] Here, the transport mechanism is based on the propagating piezoelectric fields accompanying the SAW at the speed of sound.

Most of the energy of a SAW, however, is stored in the elastic part of the wave, as the piezoelectric effect adds usually only a small contribution in the percentage range. The periodic deformation of the surface—in the case of a pure Rayleigh mode normal to the surface—can very efficiently couple to a fluid. Liquids on the surface are subject to this vibrating force and absorb parts of the energy, leading to acoustic streaming. Here, the acoustic mismatch between the fluid and the substrate leads to a diffraction of the sound wave entering the fluid. The diffraction angle is in first order approximation only determined by the ratio of the sound velocities in either material. For a strongly piezoelectric substrate such as $LiNbO_3$, for example, and water representing the liquid, a typical diffraction angle is of the order of 20°.

In Figure 16.1(a), we depict the situation for water residing on top of a $LiNbO_3$ substrate. The SAW is entering the droplet from the left. The wave fronts indicate the direction of the flow in this case. θ_R represents the diffraction or Rayleigh angle for this situation, which can easily be derived from a phase matching picture.

$$\sin(\theta_R) = \frac{v_{\text{Fluid}}}{v_{\text{SAW}}} \tag{16.1}$$

Figure 16.1(b) shows the result of a finite element calculation. Here, the actual pressure amplitudes are calculated that form the SAW induced longitudinal wave in the fluid.[15,16] Here, the SAW is considered as a series of

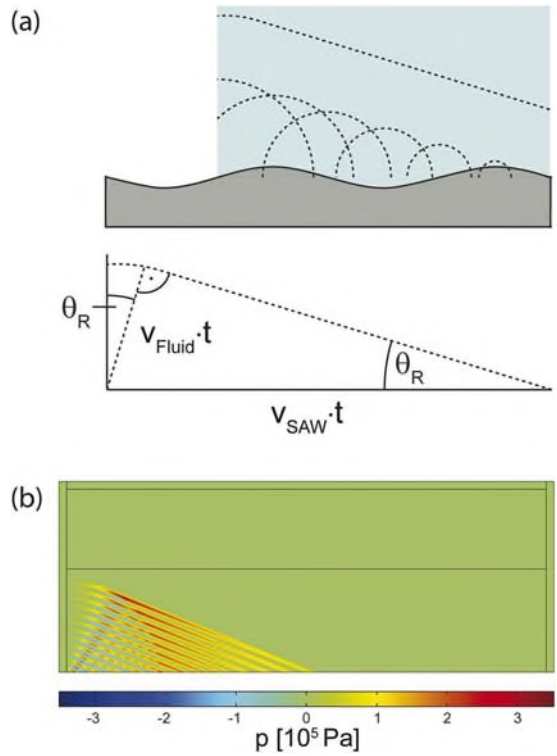

Figure 16.1 (a) Sketch of the SAW induced acoustic streaming effect. A SAW propagating at the surface of a substrate enters a region covered with a fluid. Each point at the surface is considered as a point-like pressure source (Huygens principle), creating longitudinal waves in the fluid. The diffraction angle θ_R can be simply calculated from basic geometrical considerations. (b) Result of a numerical calculation according to eqn (16.1) through eqn (16.3). Here, the SAW induced pressure wave into the fluid is shown.

point sources Q, distributed over the surface of the substrate. The pressure wave equation then reads:

$$\nabla \cdot \left(\frac{1}{\rho_i} \nabla p \right) - \frac{1}{\rho_i v_i^2} \frac{\partial^2 p}{\partial t^2} = Q \tag{16.2}$$

Here, the density and velocity in the regions of the substrate and the water, respectively are denoted by the index i. At the contact plane between water and substrate, the pressure gradient is given by the normal component of the acceleration caused by the SAW:

$$\vec{n} \cdot \nabla p = \rho_{\text{Fluid}} \omega^2 H(v_{\text{SAW}} t - y) A_0 \sin(ky - \omega t) exp(-y/\kappa_{\text{op}}) \tag{16.3}$$

Due to viscous damping, the SAW with an amplitude A_0 becomes exponentially attenuated in the fluid. The coupling constant is assumed to be κ_{op}. The Heaviside function H ensures an abrupt entrance of the SAW into the fluid, as it is assumed in our model. At the interface between substrate and fluid, continuity is ensured by

$$\vec{n}\cdot\left(\frac{1}{\rho_i}\nabla p_i - \frac{1}{\rho_j}\nabla p_j\right) = 0 \tag{16.4}$$

At low acoustic powers, the pressure gradient drives an internal acoustic streaming in the fluid. This internal flow leads to a complex streaming behavior in most cases, as the exact streaming behavior, although being completely deterministic—if diffusion is neglected for a moment—very strongly depends on the actual geometry of the problem.

16.3 Acoustically Induced Mixing

The complex streaming patterns[17] arising from the interaction between the SAW and a fluid on top of the substrate can be very efficiently used for mixing small quantities of liquid.[18] It should be noted that apart from the SAW described in this article, other acoustic mixers have also been reported.[19] All of them rely on acoustic streaming in one sense or another.

However, as the exact geometry of the flow lines and their temporal development depend on many different parameters such as geometry, viscosity, location of the fluid with respect to the IDT on the chip surface, *etc.*, it is usually not sufficient to simply subject a small quantity of liquid to a SAW on the chip. Instead, one has to make sure that the SAW–fluid interaction leads to a thorough folding of the flow lines during the mixing process. This can be achieved, for example, by either dynamically switching the frequency of the SAW (leading to different flow patterns) or by subjecting the fluid to two or more SAW beams. If those beams are modulated in time with respect to each other, an efficient folding of the flow lines can be achieved, resulting in a quasi-chaotic advection and optimal mixing behaviour.[19] This is demonstrated in Figure 16.2, where we show the flow lines in a circular water disc (confined between two solid plates) subjected to a SAW beam, coming from the right. The difference between the upper two and the lower panels is just the entry point of the SAW. Clearly, one recognizes two different flow patterns. The flow lines have been made visible by superposition of a number of video frames and fluorescent tracer particles within the liquid. The solid lines in the two panels on the right are the result of a numerical, finite element calculation and show an extremely good agreement with the experimentally obtained traces.

The extremely fast and versatile mixing properties of SAW driven microfluidic chips have recently been commercialised in a microarray hybridization chamber for biological purposes.[20,21] Here, a microarray covered with, *e.g.* single stranded DNA oligonucleotides is subjected to a thin layer of fluid

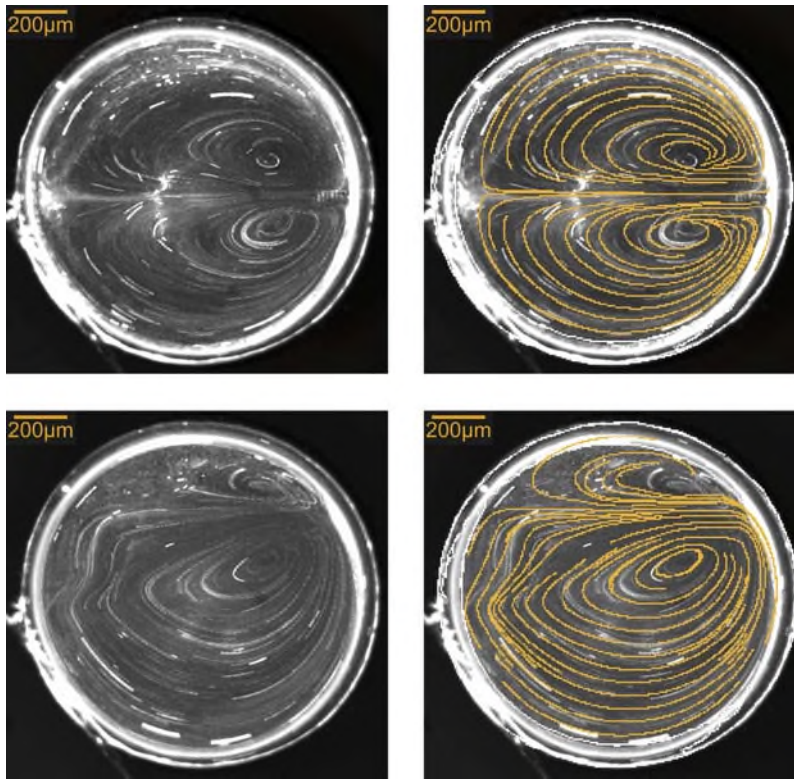

Figure 16.2 Flow lines in a flat circular water disc ($d \approx 500$ µm) confined between the piezoelectric substrate and a glass cover slide. A SAW is impinging from the right. The left panels show the experimentally obtained flow lines employing fluorescent tracer particles and video frame superposition. In the right panels the flow lines as being calculated in a numerical model have been superimposed. The upper two and the lower two panels differ by the entrance point of the SAW beams, resulting in different flow patterns. Switching between these patterns may lead to a quasi-chaotic advection.[19]

containing an unknown sample of evenly single stranded DNA. This sample is usually covered with a glass slide, confining it to a thickness of about 50 µm. The SAW induced actuation of the fluid and the folding of the flow lines induces a dramatic improvement of the hybridization speed and thus a much shorter time to the result.[21]

It is also possible to couple the SAW on the piezoelectric substrate directly through the (solid) bottom of a microfluidic device on top of the SAW chip surface. Here, the SAW first converts into a wave in the container bottom (*e.g.* a cuvette or a microtiter plate), and then enters the fluid within. Again, we observe diffraction and a resulting acoustic streaming in the miniature container. In Figure 16.3, we show such a 'separate media' coupling into the

Figure 16.3 SAW induced fluid actuation in one of the wells in a microtiter plate (left) and in a quartz cuvette (right), visualized by the agitation of some ink initially located at the bottom. In the microwell, the IDT was placed directly under the well and has been coupled through its bottom. In this case, as the IDT is completely symmetric, two jets are excited under the Rayleigh angle θ_R (Advalytix AG, unpublished).

wells of a microtiter plate (left) and into a quartz cuvette (right). Pulsed or multi frequency operation of the SAW leads to perfect mixing behavior within the wells. A detailed analysis of the temporal modulation of the SAW sources with respect to each other is given in the paper by Frommelt *et al.*[19] One important aspect for this scheme is that it does not require physical contact between the mixant and the mixer. It can be fully integrated into an analysis setup for biological assays. Also, as the SAW chip is separately coupled to the micro wells, in principle each well can be addressed individually. It is also worth mentioning that the SAW can be excited remotely by, *e.g.* inductively coupling the high frequency radiation into the IDT.

16.4 Acoustic Droplet Actuation

At higher SAW amplitudes and for isolated liquid volumes on the chip surface, an acoustically induced movement of the whole volume can be observed. First described by Shiokawa *et al.*,[22] the SAW at the surface of a (piezoelectric) substrate can strongly interact with such a droplet.[23–27] Apart from vividly bringing the droplet into rotation, its surface and thus the boundary conditions for the acoustic streaming becomes strongly distorted. At the same time, the center of mass of the droplet becomes pushed into the direction of SAW propagation and its wetting angles at the 'windward' and 'lee' side differ considerably. Both effects lead to a propulsion of the droplet into the direction of the SAW. This effect can be used for microfluidic chips, where droplets act as virtual containers and reactors at a very small scale. Surface tension makes it possible that those virtual test tubes are held together without the need for a real container. Moreover, the surface of the substrate on which the droplets are residing and acoustically actuated can be chemically functionalized in terms of the wettability properties.[24] Then,

a whole fluidic track system can be constructed on which the droplets can be moved easily. A manifold of transducers on the chip together with such a fluidic track system can be exploited as electrically addressable microfluidic processors.[28–30]

In Figure 16.4, we show the effect of an impinging SAW on a small droplet ($V \approx 50$ nl) at the surface of a $LiNbO_3$ chip. To demonstrate the strong deformation of the droplet under the influence of the SAW, we superimposed two video frames with and without the SAW induced action. Despite the fact that the back flow effects in the droplet are no longer well defined, one can easily identify the Rayleigh angle in the figure. In Figure 16.4(b), we show the result of a numerical calculation for the droplet deformation together with the internal streaming flow lines, including dynamic boundary conditions caused by the deformation of the droplet shape. This strong deformation, of course, has a back action on the internal (re-)flow, which makes the numerics quite cumbersome.[31]

The possibility to deliberately and controllably actuate small amounts of fluids along the surface of a planar substrate together with the SAW streaming mixing possibilities within the droplet make this technique extremely well suited for laboratories on a chip. The SAW are generated by IDTs, the trajectories of the droplets are predefined either by a chemical surface modification or by the shape of the SAW 'beam' normal to the propagation direction. Due to diffraction effects at the edges of the IDT aperture, the SAW wavefronts usually exhibit typical ripples normal to the propagation direction, providing a self-centering of any droplets within the propagation path. Chemical modification of the surface can be done in many different ways, the most convenient one being a laterally patterned silanization to define hydrophobic and hydrophilic regions on the chip surface. As all the technological steps to produce such SAW driven microfluidic chips

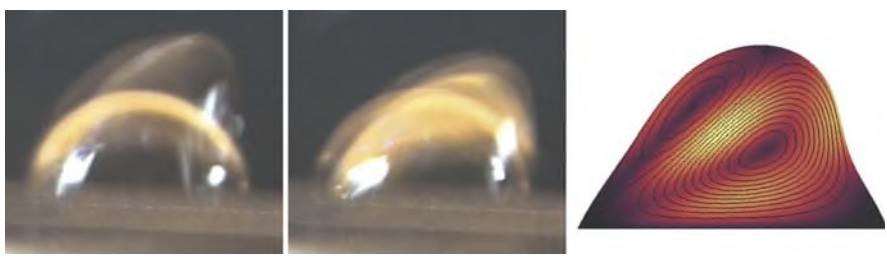

Figure 16.4 Left and center: water droplet on a $LiNbO_3$ substrate under the influence of a pulsed SAW impinging from the left. To visualize the strong deformation of its surface and shape, two video frames have been superimposed. (Advalytix AG, unpublished) Right: example for the streamlines within a droplet as the result of a numerical model. Here, the droplet is deformed only by the viscous stress at the boundary. In this example, the flow is driven by a non-conservative force density alone whereas the conservative part of the force vanishes such that the pressure is constant inside the droplet.[32]

rely on standard techniques from semi-conductor planar technology, and are all carried out at the planar surface, a more complex infrastructure is easily implemented on the surface of the same chip. This could be used to produce heaters, sensors or even micro arrays for an *in situ* control of biological assays. All the active elements on the chip are electrically controllable and can thus be run using computer software. The chips are cheap as they do not involve any complex lithography or doping *etc*. This makes them perfect candidates for single use consumables, which also excludes possible cross-contamination between different batches. All the necessary electronics are combined in an apparatus where the chip is inserted as needed. A bar code on the chip even makes it possible to tell the computer and the electronics the necessary protocol. However, as the chips might differ slightly from batch to batch due to production variances, a 'blind' operation of the protocol might lead to erratic behavior. Therefore, an active feedback of, *e.g.* the droplet position on the chip and the actuation mechanism is needed. For this purpose, a special kind of IDT proves extremely useful. Here, we employ so-called slanted transducers, where the resonance frequency changes across its aperture by varying finger spacing.[33] Thus, a spatial coordinate along the IDT aperture converts directly into a frequency. Hence, sweeping the excitation frequency for the IDT across its operation band and measuring the SAW transmission directly yields the position of a droplet in the propagation path.

In Figure 16.5, we show the result of such position detection on a chip. In the left panel, we show a picture of the chip. On the top and at the bottom of the chip, the slanted IDTs are seen; the two bright lines extending from left to right are the fluidic tracks, made visible by a metallization. On these tracks, a small droplet is moving. The right panel shows the SAW transmission between the IDTs as a function of the excitation frequency, exhibiting a strong absorption over a specific frequency band that can be identified with a specific location on the chip. The same idea has also been followed by other groups[35] and is well established for the active position control of small droplets on acoustically driven microfluidic chips.

16.5 PDMS Microfluidics

Since the versatility of PDMS was demonstrated by Whitesides about a decade ago,[36–39] formation of microfluidic devices in a process called soft lithography has revolutionized fabrication.[40,41] In a rapid prototyping process, this method allows minimization of operating time from concept to experiment. The unique features of PDMS, among which are excellent optical transparency, good biocompatibility enhanced by high permeability to oxygen and carbon dioxide, low toxicity and elastic behavior, have permitted a number of novel approaches and applications. To a large extent, the rapid development of microfluidics was made possible utilizing PDMS technology. Therefore, to take advantage, it is useful to integrate novel designs of experiments and applications into the large number of features that have been realized and developed in PDMS based fluidics.

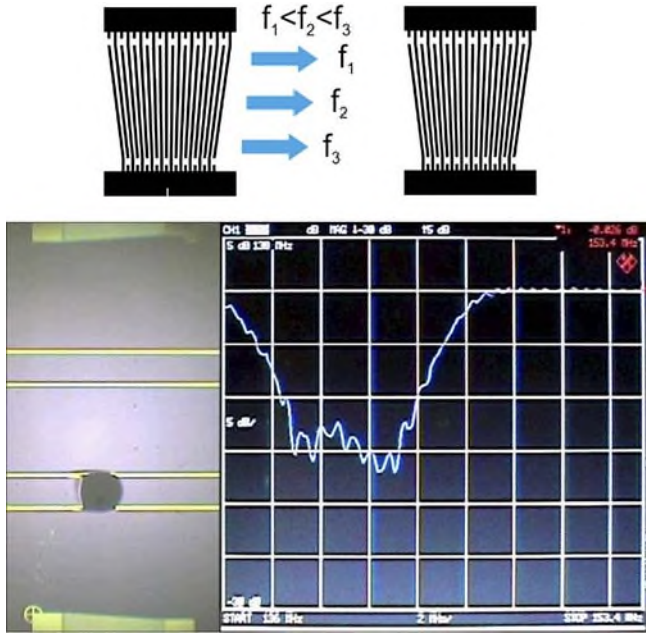

Figure 16.5 Top: slanted IDT for droplet detection on a chip.[33] The transducer fingers have varying spacing along the aperture, leading to a location dependent SAW resonance frequency. Sweeping the excitation frequency over the transmission bandpass leads to the excitation of a narrow ($\approx 10\ \lambda$) SAW beam at a specific location. Bottom left: photograph of the chip with a droplet on it. On the top and at the bottom one can see the slanted transducers whose transmission is monitored while the droplet is moving across the sound path. The horizontal lines indicate the position of fluidic tracks, fabricated by a modulation of the surface energy and made visible by metallization. Right: oscilloscope trace of the SAW transmission between the two slanted transducers as a function of frequency. Over the frequency band corresponding to the position and size of the droplet, one observes a pronounced SAW attenuation that can be used for position feedback control on the chip.[34]

The SAW–PDMS hybrid technique combines the advantages of both technologies to provide a low cost and very versatile platform for manipulation of small amounts of fluids in a closed system, minimizing contamination.

16.5.1 SAW Excitation on a Piezosubstrate and Acoustic Coupling to Standard PDMS Devices

Fabrication and mounting of the acoustic hybrid devices is very simple and involves only a few extra steps in addition to standard PDMS procedures. However, the SAW actuating chip has to be produced in advance. This chip consists of two components. The acoustic part is composed of a piezoelectric

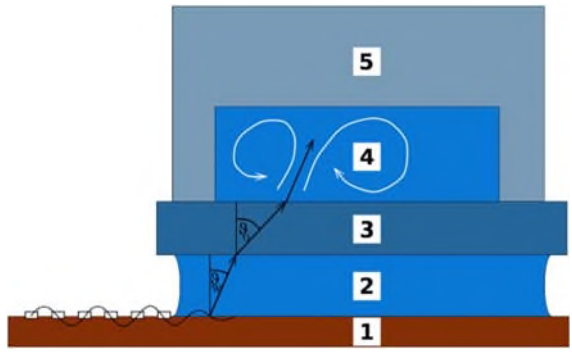

Figure 16.6 Top: side view sketch of the path of the acoustic wave coupling into the channel: a surface acoustic wave is excited by the IDT and travels along the lithium niobate substrate (1). It is refracted into a longitudinal wave in the coupling liquid (water) (2) at a Rayleigh angle $\theta_W = 21.8°$ while the surface wave on the substrate is attenuated on a characteristic length scale of 325 μm. The longitudinal acoustic wave passes through the 150 μm thick water layer and is subsequently refracted into a transversal wave in the glass cover slide at a Rayleigh angle of $\theta_G = 54.4°$. At the top of the glass slide, the wave is refracted again, enters the water-filled channel (4) and transfers momentum to the liquid, causing acoustic streaming as indicated, before it couples into the PDMS layer on top where it is further attenuatued (reproduced from ref. 58 with permission).

substrate with interdigitated electrodes to electrically excite the mechanical surface acoustic wave as described before. The other component is the PDMS channel that can be either directly bonded to the piezo-chip using ozone plasma etching or coupled to the chip after bonding to a glass substrate. Although the former geometry provides a closer coupling by minimization of chip–fluid distance, it requires full assembly of the chip for each experiment. Coupling a standard PDMS–glass device to the acoustic chip enables the reuse of the piezo-chip and saves assembly time. Several PDMS–glass channels may serve as disposables and can be used one after another simply by placing them onto the piezo-chip.

However, the acoustic contact between the PDMS–glass and the chip has to be enabled by a contact liquid and is critical for the robustness and efficiency of the hybrid device. A schematic of the setup is shown in Figure 16.6. When a microfluidic channel is placed on top of the substrate, the Rayleigh wave generates an acoustic wave that couples through the intermediate coupling liquid, for example a water layer, and through the glass bottom of the channel into the fluid, transferring momentum along the direction of propagation and ultimately inducing fluid streaming. Depending on the geometry of the confining PDMS channel in the actuation region, this may create several flow vortices[42] but also may induce a directed flow as is demonstrated in the subsequent paragraph. The flow velocity can be easily controlled electronically by the SAW power.

16.5.2 Pumping in Closed PDMS Channels

Pumping fluid in microfluidic devices is a delicate issue because it often involves an interface between an external pump and the fluid channel. Probably most often used in microfluidics are syringe pumps to drive fluid at a certain volume rate through the device or alternatively, an external pressure applied *via* tubing connection pushes the flow. Both mechanisms suffer from the risk of a leaking connection, in particular when highly complex chip designs involve a large number of pumps. Furthermore, response times in these systems can be as high as several tenths of seconds making it impossible to control a non-stationary flow, for instance to mimic the pulsative flow of a heartbeat.

Although there are several other types of pumps exploiting various physical effects including electrokinetic and electro-osmotic pumps, these pumps have a low pumping efficiency or depend on the fluid properties such as the electrolyte concentration of the liquid. Using multi-layered soft lithography using PDMS to form a peristaltic pump similar to Quake-valves provides faster response times but it needs to be connected to external air pressure generators. Surface acoustic wave actuated pumping avoids these disadvantages by fully integrating the pump and the fluidic chip.

The electrical connections to drive the surface wave can be implemented onto the chip using vapour deposited conductive paths. The actuation principle of acoustic streaming is independent of pH and electrolyte concentration and uses low voltages, which is important when pumping biological samples and to avoid electrochemical effects. Moreover, the method allows the continuous actuation of non-stationary fluid flow with fast response times. A unique feature of the acoustically driven pumps is the opportunity to pump in closed looped channels without the need for fluid inlets or outlets. Issues of cross-contamination can therefore be effectively addressed and looped channel structures for chemical incubation can be envisioned. An example of such a closed loop channel geometry is shown in Figure 16.7. In such geometries, typically, flow velocities in the range of $0 < v_m < \sim 1$ cm s^{-1} can be achieved. Therefore, the flow is laminar all over the microchannel because the Reynolds number is still low ($Re < 10$) at all positions. We determined the flow velocity in the straight channel of Figure 16.7 using particle tracking techniques at different channel heights and compare in Figure 16.8 the velocities obtained to the theoretical flow profile of a rectangular pressure driven channel.[43]

The plot of both the experimentally measured and the theoretically calculated curve are in excellent agreement demonstrating that the acoustic streaming builds up an effective pressure that drives the fluid flow. In other words, the stationary velocity flow profile can be simply calculated by solving the incompressible Stokes equation with a driving pressure specified by the power of the acoustic actuation and the boundary condition of the constrained channel geometry. This allows the simulation of more complex flow situations and microfluidic channel designs with standard techniques such as commercially available finite element methods.

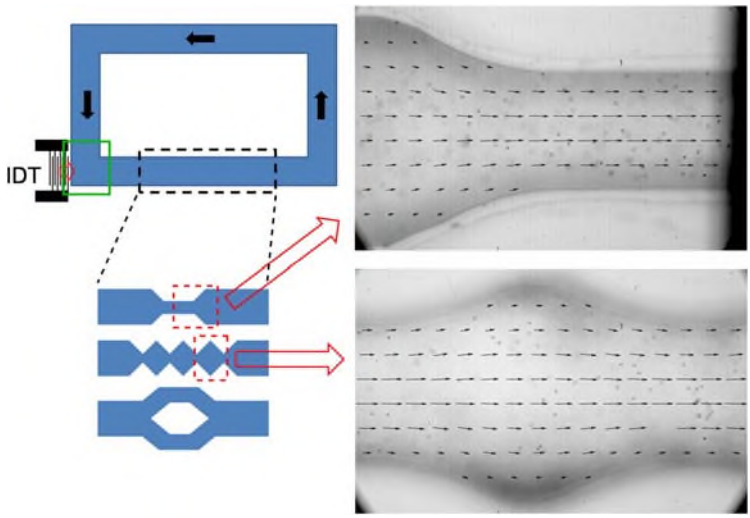

Figure 16.7 Left: schematic of the hybrid PDMS–SAW chip as seen from above. The basic channel (width = 1 mm, height = 0.75 mm, loop circumference = 42 mm) consists of a closed rectangular PDMS channel and is bonded onto a glass substrate. The IDT is carefully positioned below the channel and pumps the fluid all around the closed channel without inlets or outlets (black arrows indicate flow direction). The IDT consists of 42 fingers and has an aperture of 624 μm and a length of 1233 μm. It is positioned in parallel to the fluid channel exactly at the PDMS–fluid boundary. Enclosed by a green line is the coupling region of the acoustics to the fluid. We have used different channel designs as indicated by the channel sections in the schematic below: a narrowing nozzle-like channel, an oscillating zig-zag channel and a bifurcated channel. Right: micrographs of the different channels are superposed with the experimentally measured flow velocity vectors (black arrows) as obtained from particle tracking with focus in the symmetry plane, *i.e.* middle of the channel. (reproduced from ref. 58 with permission).

For non-stationary flows, the response time of the system has to be taken into account. As pointed out by Stone[44] for syringe pumps, compressibility of the fluid and small air bubbles in the fluidic system can seriously affect the response time. Even without bubbles this transient time can reach values of a minute before a stationary flow has been established, a fact many experimentalists are aware of. The highest oscillation frequency for a non-stationary flow that is accessible to a system is given by the inverse of the response time η. We have determined the response time for the aforementioned straight channel geometry by applying a square wave modulated HF signal to the IDT electrodes and observed the corresponding flow relaxation for different values of the channel dimensions (Figure 16.9). The measured response times are well below 100 ms that correspond to a maximal oscillation frequency of 10 Hz. For physiologically relevant situations such as the pulsative flow of the heartbeat, a typical frequency of $\sim$1 Hz is observed.

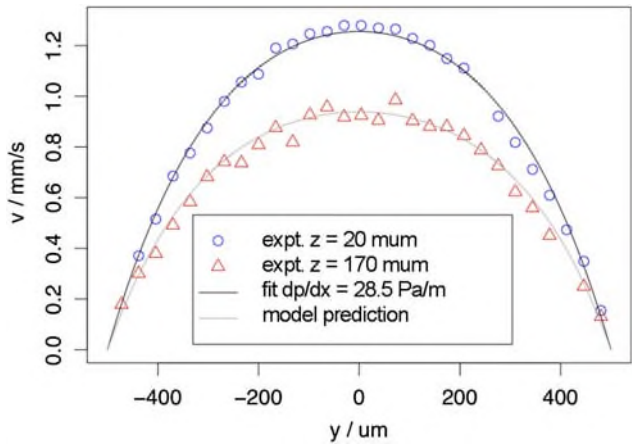

Figure 16.8 Left: flow profile as being measured in the PDMS channel (basic rectangular channel as shown in Figure 16.7; width = 1000 μm, height = 750 μm). The fluid moves in the x-direction, y is the horizontal and z is the vertical direction. The origin of the coordinate system is at the center of the channel. Blue circles represent the flow velocity measured near the channel center ($z = 20$ μm), red triangles show the velocity measured at $z = 170$ μm. The black line is a fit of the analytical model to the measurement at $z = 20$ μm (blue circles) and yields a pressure gradient $G = \mathrm{d}p/\mathrm{d}x = 28.5$ Pa m^{-1} as a free fitting parameter. The dashed line shows the prediction of the analytical model for off-center flow ($z = 170$ μm) using G as determined above. This is in good agreement with measurements (red triangles). Reproduced from ref. 58 with permission.

Hence, with the acoustic pump, a simple platform to mimic blood flow in small capillaries can be envisioned. Together with the biocompatibility of PDMS and the opportunity of cell growth on its surface, a simplified model of a blood vessel under realistic flow conditions can be obtained.

16.5.3 Droplet Based Fluidics

Although favorable in some cases, one-phase microfluidics as demonstrated in the previous paragraph inherently suffers from defining and manipulating distinct volumes of fluids,[45] which is a considerable prerequisite for many applications. Firstly, the integrity of a defined liquid volume disperses simply because diffusion becomes significant on the micron length scale. Secondly, in microchannels, which are widely used, the parabolic flow velocity profile of a pressure driven flow enhances mixing by Taylor dispersion.[46,47] Even though the latter can be circumvented using electro-osmotically driven flows generating a plug flow profile, these problems are still an important issue. Both problems can be avoided using droplet fluidics.[48] In droplet fluidics, emulsion droplets are employed to define liquid containers of picolitre volume.

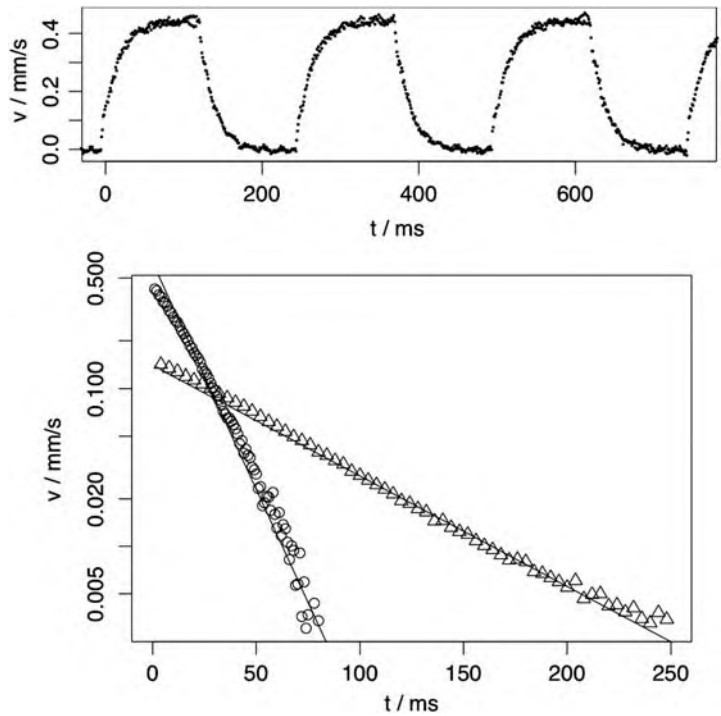

Figure 16.9 Response of the flow velocity to a 2 Hz square-wave modulation of the SAW (20.5 mW, 13.1 dBm). The top right inset shows the time-dependent flow velocity of a 4 Hz modulation in a smaller channel (63.5 mW, 18.0 dBm). After repeated voltage cut-off, the flow velocity decays exponentially. The plot below shows on a logarithmic scale the decay in two different channels both of height $h = 0.75$ mm and a width of 1 mm and 0.5 mm, respectively. The exponential fits result in a decay time $\tau = 61.7 \pm 0.4$ ms for the wider channel and a decay time $\tau = 15.1 \pm 0.4$ ms for the smaller channel (reproduced from ref. 58 with permission).

These containers can be utilized to encapsulate reactants, cells, bacteria or polymers such as DNA or proteins. They provide a unique microenvironment and inhibit diffusive as well as convective mixing. Precise control of droplet volume in combination with coalescence and splitting of drops enables many analytical applications and can be regarded as digital microfluidics, like the single phase droplets described earlier. Droplet formation is driven by interfacial tension and can occur right at the tip of the capillary orifice (dripping) or further downstream by disintegration of the fluid jet (jetting). The two regimes can be characterized by the capillary number of the outer fluid and the Weber number of the inner fluid.[49,50] An alternative method for droplet production in glass capillaries is the formation in a microchannel formed by the elastomer PDMS.[51] Both of these techniques allow for serial production of multiple emulsions of higher order and hierarchy. In multiple

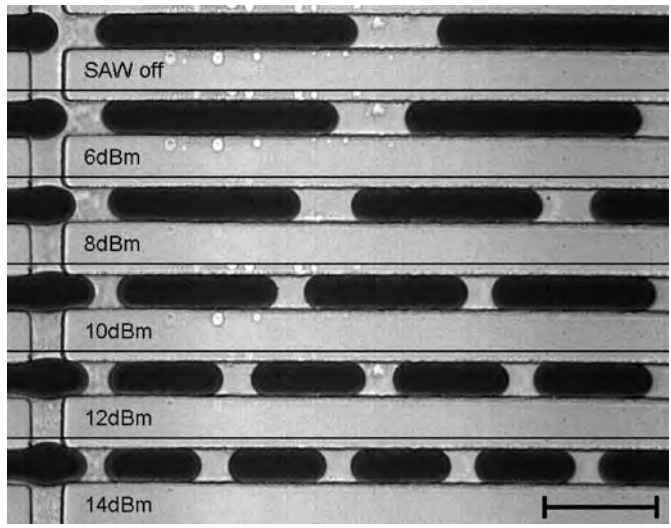

Figure 16.10 Drop formation in a flow focusing geometry. Stack of a dropmaker cross-junction driven at different acoustic powers. Upper image: in the absence of an acoustic field, drops break up at the junction forming extended fluid drops. Lower images: depending on the power, the time for drop formation can be decreased, causing drops of shorter length (reproduced from ref. 51 with permission).

emulsions, the emulsion drops themselves contain a controlled number of drops. Double emulsions in particular are useful in vesicle preparation[48] that can be applied to encapsulate reagents or magnetic beads.

Although drops can be produced at rates as high as several kHz by changing the flow rates of the dispersed and continuous phase, transients can be extreme.[44] For a syringe driven system, equilibration times can already reach several minutes. This seriously limits the controllability of the dropmaker and the fast production and processing of well-defined drop volumes.

Very recently, we have demonstrated that this limitation can be overcome by using SAWs. In a flow-focusing device we actively control the volume of each drop in real time.[51] The intensity of the acoustic field regulates the dimensions of the drops as shown in Figure 16.10.

Pinch-off occurs in the so-called squeezing-regime[52,53] of drop formation. In this regime we have demonstrated that the length of drops can be described using a linear model with a constant slope $\partial l/\partial P_{SAW}$ of drop length l on SAW power P_{SAW} The fast response times and precise control allow a fully electronically controlled way of drop formation in real time. A similar approach can be followed using a T-junction geometry; see Figure 16.11.

The rapid development of biomedicine and diagnostics creates a great demand for high throughput systems to analyze tiny amounts of biofluids, a goal that can be achieved by applying droplet based fluidics in PDMS designed devices. However, this requires ultrafast processing techniques to

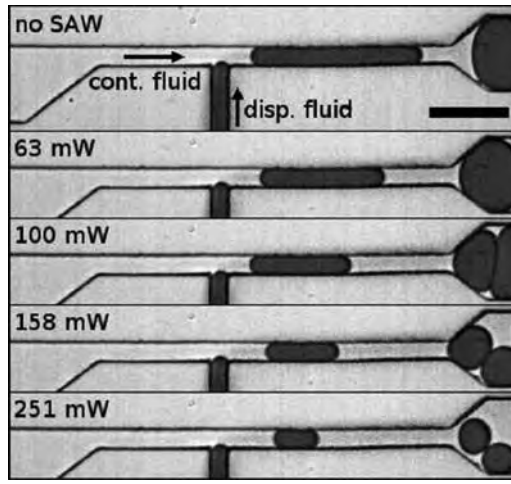

Figure 16.11 Dropmaker T-junction. The continuous fluid (oil) enters from the left, the dispersed aqueous fluid from the bottom, where it breaks up into droplets that flow to the right. The scale bar denotes 100 μm. The images show the droplet length at different SAW powers while the external pressure of the inlets was held constant at 5.7 kPa (continuous fluid) and 11.7 kPa (dispersed fluid) (reproduced from ref. 59 with permission).

manipulate drops and cells on the chip. The available state of the art techniques suffer from low processing rates or a dependence of sorting efficiency on the properties of the objects (droplets, cells) to be processed. For example, switching valves are limited to frequencies of ~10 Hz and techniques based on dielectrophoresis clearly depend on the contrast of permittivity between continuous fluid and objects. Both restrictions can be overcome using a surface acoustic wave based technique. SAW actuated droplet and cell direction allow us to sort cells to rates of up to ~10 kHz. To demonstrate the superior control of droplets, we integrated a microfluidic drop maker and the acoustic chip on a PDMS device. The acoustic part consists of a channel that splits into two outlet channels. Adjacent to the sorting region and just before the branching, an IDT is positioned that creates acoustic streaming to laterally deflect the droplets, as shown in Figure 16.12, and direct them into either one of the outlet channels. The droplets are aqueous drops suspended in an immiscible continuous environment that consists of HFE-7500 fluorocarbon oil with 5% (vol/vol) 1*H*,1*H*,2*H*,2*H*-perfluoro-1-octanol, stabilized by 1.8 wt% of the fluorosurfactant ammonium carboxylate of DuPont Krytox 157. The same principle can be applied to hydrogel particles that provide a significantly lower contrast when suspended in water. Therefore, we have synthesized PAM particles using microfluidic droplet polymerization in a separate PDMS device. We added 10% of the acrylamide monomer as well as 10% of the cross-linker BIS-acrylamide to the middle channel, while oil flowed through the two side channels. The particles were then suspended in

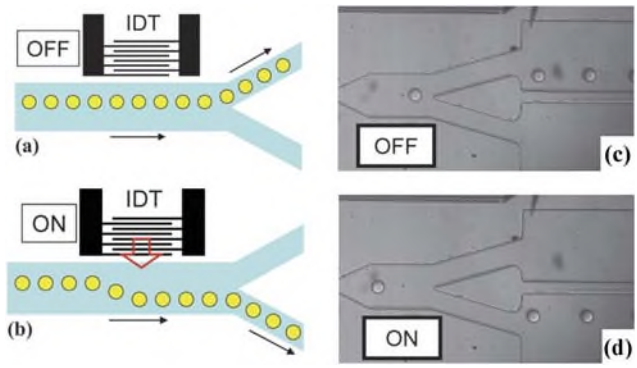

Figure 16.12 (a) and (b): Schematic of the hybrid PDMS–SAW chip as seen from above: a branched PDMS channel is coupled to a SAW device. (a) If the SAW power is switched off, all drops flow along the upper channel because of its lower flow resistance. (b) If the SAW power is switched on, the acoustic streaming induced by the IDT (red arrow) drives the droplets in the lower channel of the branch. (c), (d): Top view of the hybrid device showing a branched PDMS channel. Monodisperse water droplets are entering at constant separation from the left and are produced further upstream in a nozzle combining oil and water inlets (not shown here). The IDT is positioned below the PDMS and is carefully aligned parallel to the channel and can be partly seen at the top of the images (dark horizontal lines). The dark tip on the right side of the IDT is a feature to facilitate alignment and should roughly aim at the upper left corner of the upper outlet reservoir. However, a misalignment of approximately 100 mm did not affect the ability to direct the drops in our experiments. (c) When the SAW is switched off, all the drops take the upper outlet channel because its cross-section is designed to be slightly larger. (d) When a RF signal of approximately 10 dBm is applied to the IDT, all drops are pushed into the lower channel. The device is 50 mm high and 100 mm in width right before the branch. Flow rates were 100 ml h^{-1} for the dispersed phase and 1000 ml h^{-1} for the continuous phase. (Reproduced from ref. 57 by permission).

water and introduced into the sorting device. Again, we were able to control the gel particle flow by application of the SAW.

Cell sorting at high rates is a problem that has been addressed often in microfluidic systems because cell populations typically possess a natural distribution of single cell properties or dimensions. Since most physical actuation mechanisms used for cell deflection and sorting directly exploit the cell's properties, the deflection effect varies within a cell population. This problem can be avoided using highly monodisperse droplets as templates for cell encapsulation.[55] However, loading drops with discrete objects such as cells or particles obeys Poisson statistics and yields many unloaded and multiply-loaded droplets. This disadvantage can be avoided to some extent using close-packed deformable particles.[52] Moreover, SAW based flow

direction steering enables cell sorting that operates in continuous flow without the need for encapsulation prior to sorting. Using the acoustic streaming technique, we are able to deflect cells directly from the bulk solution such as cell buffer or blood plasma. The sorting principle is independent of the cell's size or properties and can operate at sorting rates as high as several kHz.[53] To minimize accidental sorting of multiple cells at the same time (Poisson statistics) and to ensure a serial flow of one at a time, we align cells by hydrodynamic focusing using a sheath flow of the cell buffer solution. When entering the focusing region, cells are accelerated and accordingly their cell to cell distance increases reducing erroneous collective sorting. Sheath and cell flow rates can be controlled in a running experiment.

Using this acoustic device, we have successfully directed various cell types including MV3 melanoma cells, murine fibroblasts and HaCaT cells. Because of the inherently small shear stress of this method, the viability of sorted cells was excellent as has been proven by viability tests.[53,54]

16.6 Conclusions

We have shown that acoustic streaming induced by surface acoustic waves is a versatile tool for microfluidics enabling superior control of small fluid volumes. It can enhance mixing in tiny volumes such as nl drops or the actuation of a droplet container on a chip substrate surface. Moreover, the technology is compatible with the widely used PDMS soft lithography. This combination allows for high throughput applications such as cell and droplet sorting at rates of $\sim 10^4$ drops per second. Its ability to pump fluid in a closed loop channel without external tubing connections is useful for cell assays that need repeated incubation periods.

References

1. N.-T. Nguyen, S. T. Wereley, *Fundamentals and applications of microfluidics*, Artech House, 2002.
2. G. Fuhr, T. Schnelle and B. Wagner, *J. Micromech. Microeng.,* 1994, **4**, 217.
3. A. Hatch, A. E. Kamholz, G. Holman, P. Yager and K. F. Böhringer, *J. Microelectromech. Syst.,* 2001, **10**, 2.
4. M. Inganas, H. Derand, A. Eckersten, G. Ekstrand, A. K. Honerud, G. Jesson, G. Thorsen, T. Soderman and P. Andersson, *Clin. Chem.,* 2005, **51**, 1985.
5. W. J. J. Welters and L. G. J. Fokkink, *Langmuir,* 1998, **14**, 1535.
6. C. Eckart, *Phys. Rev. Lett.,* 1948, **73**, 68.
7. W. L. Nyborg, Acoustic streaming, in *Physical Acoustics*, ed. W. P. Mason, Academic Press, 1965, vol. 2B, pp. 265–330.
8. L. J. W. S. Rayleigh, *Proc. London Math. Soc.,* 1885, **17**, 4.
9. (a) A. A. Oliner, *Acoustic Surface Waves*, Springer, 1973; (b) H. Matthews, *Surface Wave Filters*, Wiley, 1977.

10. D. S. Ballantine Jr, R. M. White, S. J. Martin, A. J. Ricco, G. C. Frye, E. T. Zellars and H. Wohltjen, *Acoustic Wave Sensors—Theory, Design, and Physico-Chemical Applications*, Elsevier, 1997.
11. A. Wixforth, M. Wassermeier, J. Scriba, J. P. Kotthaus, G. Weimann and W. Schlapp, *Phys. Rev. B,* 1989, **40**, 7874.
12. (a) R. M. White and F. W. Voltmer, *Appl. Phys. Lett.,* 1965, **7**, 12; (b) D. P. Morgan, Rayleigh Wave Transducers, in *Rayleigh-Wave Theory and Application*, ed. E. A. Ash and E. G. S. Paige, Springer, 1985.
13. C. Rocke, S. Zimmermann, J. P. Kotthaus, G. Böhm and G. Weimann, *Phys. Rev. Lett.,* 1997, **78**, 4099.
14. C. Wiele, F. Haake and A. Wixforth, *Phys. Rev. A,* 1998, **58**, R2680.
15. T. Frommelt, D. Gogel, M. Kostur, P. Talkner, P. Hänggi and A. Wixforth, *IEEE Trans. Ultrason. Ferroelectr. Freq. Control,* 2008, **55**, 2298.
16. H. Antil, R. Glowinski and R. H. W. Hoppe, *et al., J. Comput. Math.,* 2010, **23**, 149.
17. Z. v. Guttenberg, A. Rathgeber, S. Keller, J. O. Rädler, A. Wixforth, M. Kostur, M. Schindler and P. Talkner, *Phys. Rev. E,* 2004, **70**, 056311.
18. K. Sritharan, C. J. Strobl, M. F. Schneider, A. Wixforth and Z. v. Guttenberg, *Appl. Phys. Lett.,* 2006, **88**, 054102.
19. T. Frommelt, M. Kostur, M. Wenzel-Schäfer, P. Talkner, P. Hänggi and A. Wixforth, *Phys. Rev. Lett.,* 2008, **100**, 034502.
20. A. Tögl, R. Kirchner, C. Gauer and A. Wixforth, *J. Biomol. Tech.,* 2003, **14**, 197.
21. Z. v. Guttenberg, H. Mueller, H. Habermueller, A. Geisbauer, J. Pipper, J. Felbel, M. Kielpinski, J. Scriba and A. Wixforth, *Lab Chip,* 2005, **5**, 308.
22. S. Shiokawa, Y. Matsui and T. Ueda, *Proc. - IEEE Ultrason. Symp.,* 1989, 643.
23. A. Wixforth, *Superlattices Microstruct.,* 2003, **33**, 389.
24. A. Wixforth, C. J. Strobl, C. Gauer, A. Tögl, J. Scriba and Z. v. Guttenberg, *Anal. Bioanal. Chem.,* 2004, **379**, 982.
25. T. D. Luong and N. T. Nguyen, *Micro Nanosyst.,* 2010, **2**, 239.
26. L. Y. Yeo and J. R. Friend, *Biomicrofluidics,* 2009, **3**, 012002.
27. A. Renaudin, P. Tabourier, V. Zhang, J. C. Camart and C. Druon, *Sens. Actuators, B,* 2006, **113**, 389.
28. C. J. Strobl, Z. v. Guttenberg and A. Wixforth, *IEEE Trans. Ultrason. Ferroelectr. Freq. Control,* 1432, **51**.
29. Z. v. Guttenberg, H. Müller, H. Habermüller, A. Geisbauer, J. Pipper, J. Felbel, M. Kielpinski, J. Scriba and A. Wixforth, *Lab Chip,* 2005, **5**, 308.
30. S. Thalhammer, in SPIE Microtechnologies for the New Millennium, *Proc. SPIE*, 2009, **7364B**, doi: 10.1117/12.820942.
31. M. Schindler, P. Talkner and P. Hanggi, *Phys. Fluids,* 2006, **18**, 103303.
32. M. Schindler, PhD Thesis (Dissertation), University of Augsburg, 2006.
33. M. Streibl, A. Wixforth, J. P. Kotthaus, A. O. Govorov, C. Kadow and A. C. Gossard, *Appl. Phys. Lett.,* 1999, **75**, 4139.
34. T. Frommelt, PhD thesis (dissertation), University of Augsburg, 2007.
35. T. T. Wu and I. H. Chang, *J. Appl. Phys.,* 2005, **98**, 1.

36. Y. Xia and G. M. Whitesides, *Angew. Chem. Int. Ed.,* 1998, **37**, 550–575.
37. G. M. Whitesides, E. Ostuni, S. Takayama, X. Jiang and D. E. Ingber, *Annu. Rev. Biomed. Eng.,* 2001, **3**, 335–373.
38. Y. Xia and G. M. Whitesides, *Annu. Rev. Mater. Sci.,* 1998, **28**, 153–184.
39. G. M. Whitesides, *Nature,* 2006, **442**, 368–373.
40. J. C. McDonald and G. M. Whitesides, *Acc. Chem. Res.,* 2002, **35**, 491–499.
41. Dong Qin, Younan Xia and G. M. Whitesides, Soft lithography for micro- and nanoscale patterning, *Nat. Protoc.,* 2010, **5**, 491–502.
42. T. Franke, S. Braunmüller, T. Frommelt and A. Wixforth, *Proc. SPIE,* 2009, **7365**, 73650O.
43. P. Tabeling, *Introduction to Microfluidics*, Oxford University Press, USA, 2005.
44. H. A. Stone, A. D. Stroock and A. Ajdari, *Annu. Rev. Fluid Mech.,* 2004, **36**, 381–411.
45. R. F. Ismagilov, A. D. Stroock, P. J. A. Kenis, G. Whitesides and H. A. Stone, *Appl. Phys. Lett.,* 2000, **76**, 2376.
46. R. F. Ismagilov, *Angew. Chem. Int. Ed.,* 2003, **42**, 4130–4132.
47. H. Song, J. D. Tice and R. F. Ismagilov, *Angew. Chem.,* 2003, **115**, 792–796.
48. R. K. Shah, H. C. Shum, A. C. Rowat, D. Lee, J. J. Agresti, A. S. Utada, L.-Y. Chu, J.-W. Kim, A. Fernandez-Nieves, C. J. Martinez and D. A. Weitz, *Mater. Today,* 2008, **11**, 18–27.
49. A. S. Utada, L. Y. Chu, A. Fernandez-Nieves, D. R. Link, C. Holtze and D. A. Weitz, *MRS Bull.,* 2007, **32**, 702–708.
50. A. S. Utada, A. Fernandez-Nieves, J. M. Gordillo and D. A. Weitz, *Phys. Rev. Lett.,* 2008, **100**, 014502–014504.
51. L. Schmid and T. Franke, *Lab Chip,* 2013, **13**, 1691–1694.
52. P. Garstecki, H. A. Stone and G. M. Whitesides, *Phys. Rev. Lett.,* 2005, **94**, 164501.
53. A. R. Abate, A. Rotem, J. Thiele and D. A. Weitz, *Phys. Rev. E,* 2011, **84**, 1–5.
54. L. Schmid, D. A. Weitz and T. Franke, *Lab Chip,* 2014, **14**, 3710–3718.
55. A. R. Abate, C. H. Chen, J. J. Agresti and D. A. Weitz, *Lab Chip,* 2009, **9**, 2628–2631.
56. T. Franke, S. Braunmüller, L. Schmid, A. Wixforth and D. A. Weitz, *Lab Chip,* 2010, **10**, 789–794.
57. T. Franke, A. R. Abate, D. A. Weitz and A. Wixforth, *Lab Chip,* 2009, **9**(18), 2625.
58. L. Schmid, A. Wixforth, D. A. Weitz and T. Franke, *Microfluid. Nanofluid.,* 2011, **12**(1), 229.
59. L. Schmid and T. Franke, *Appl. Phys. Lett.*, **104**(13), 133501.